Infrared Reflection−Absorption Spectroscopy and Density Functional Theory Investigations of Ultrathin ZnO Films Formed on Ag(111)

Mie Andersen,*,§,† Xiaojuan Yu,§,‡ Matthias Kick,† Yuemin Wang,*,‡ Christof Wöll,‡ and Karsten Reuter†

†Chair for Theoretical Chemistry and Catalysis Research Center, Technische Universität München, Lichtenbergstraße 4, 85747 Garching, Germany

‡Institute of Functional Interfaces, Karlsruhe Institute of Technology, Hermann von Helmholtz Platz 1, 76344 Eggenstein Leopoldshafen, Germany

ABSTRACT: Reactivity at metal oxide interfaces is of fundamental importance in heterogeneous catalysis. Herein, we report a thorough surface science study on the growth and chemical activity of ultrathin ZnO films on Ag(111) by grazing emission X ray photoelectron spectroscopy and temperature dependent infrared reflection−absorption spec troscopy using CO as a probe molecule. Compared to bilayer ZnO on Cu [Schott, V.; *Angew. Chem. Int. Ed.* **2013**, 52, 11925−11929], we find a much decreased CO binding energy of 0.24 eV for bilayer ZnO on Ag. Furthermore, the anomalous, substantial red shift of the CO stretch frequency with respect to the gas phase value identified for ZnO/Cu is absent in the ZnO/Ag system, where we instead report a slightly blue shifted frequency at 2146 cm^{-1} for isolated CO molecules. In order to interpret these differences of ZnO thin layer supported on these two coinage metals, we carried out a thorough theoretical analysis using density functional theory calculations employing van der Waals corrected generalized gradient approximation (GGA) type and hybrid functionals. We show that bilayer ZnO forms a flat graphitic like structure on Ag in contrast to the previously reported strongly corrugated ZnO film formed on Cu. While our results show that GGA type functionals cannot in general be applied uncritically for CO adsorption on ZnO, we explicitly validate our results for the ZnO/Ag system by comparison to hybrid functional calculations for selected model systems.

1. INTRODUCTION

The tendency of certain oxides to wet the surfaces of metals has been intensively studied, both as carefully prepared model systems for surface science investigations as well as in the context of their spontaneous formation in real catalytic systems.[1−7] While such oxidic thin films often cause an undesired blocking of active metal sites, they have in several cases been shown to contribute beneficially toward the stability, selectivity and/or activity of catalysts.[2−5] The unusual proper ties of ultrathin metal−supported oxide films have been interpreted in terms of their significantly altered structure and adsorptive properties compared to the bulk oxide[1] as a consequence of strong metal−support interactions (SMSI).

Among the studied catalytic systems exhibiting SMSIs, ultrathin films of zinc oxide on metals have received particular attention owing to their potential importance and applications as catalysts for methanol synthesis, the water gas shift reaction, and CO oxidation.[2,8−14] Whereas bulk ZnO crystallizes in the wurtzite structure, thin films of this interesting oxide have been predicted to form layered, graphitic structures, ZnO$_{(gr)}$, with a layer stacking as in h BN.[15] Previously, we have shown that a thin ZnO film grown on brass(111) adopts a distorted structure in between the ideal wurtzite (0001) and the planar ZnO$_{(gr)}$ structure.[10] It was found that this new thin film phase of ZnO exhibits Zn atoms with a lowered oxidation state, which significantly enhanced the bonding of CO to the film. As a fingerprint of the modified chemical reactivity of the film, an anomalous red shift by about 70 cm^{-1} relative to the normal stretch frequency for CO adsorbed on wurtzite ZnO was observed. Interestingly, a similar red shift has recently been observed in an industrial type Cu/ZnO catalyst for methanol synthesis from CO$_2$ and H$_2$.[11] This CO frequency was assigned to an adsorption site characterized by a partial coverage of the copper nanoparticles in the catalyst by a thin layer of metastable, defective zinc oxide, similar to the model catalyst investigated in ref 10, and in agreement with previous

observations of such structures in industrial type Cu/ZnO catalysts by transmission electron microscopy (TEM).[9]

Apart from the catalytic applications of ultrathin ZnO films on metals, it is also of fundamental interest to understand the origins of their modified adsorptive properties and in particular the role of the underlying metal substrate. In addition to ZnO films grown on Cu,[10,16] the growth on a number of other metallic substrates has also been realized, including Ag,[17−19] Au,[20,21] Pt,[12] and Pd.[22] The role of the metal substrate for the structure of thin ZnO films has been studied in great detail using density functional theory (DFT).[23] The DFT results from ref 10 demonstrated that ZnO on Cu(111) exhibits a substantial corrugation, whereas it was found that on more noble metals such as Ag the ZnO film is almost flat. On Ag(111), combined scanning tunnelling microscopy (STM) and surface X ray diffraction (SXRD) experiments have revealed that ZnO films transform to a more corrugated wurtzite like structure in the 3−4 monolayer (ML) range and that incomplete layers begin to form for thicknesses above 2 ML.[19] DFT studies of such islands of ZnO in the 3−4 ML range on top of a closed 2 ML film on Ag(111) showed that the islands undergo a structural transition to the wurtzite structure in the core of the island, whereas the edges and corners of the islands are characterized by reconstructions.[24]

In this contribution, we study the role of the underlying metal substrate for the chemical activity of ultrathin films of zinc oxide. Compared to our previous measurements carried out using a CuZn (brass) substrate,[10] we here concentrate on ZnO grown on an AgZn substrate. The growth process is investigated as a function of the O_2 exposure and the oxidation temperature by grazing emission X ray photoelectron spectros copy (XPS) and temperature dependent infrared reflection− absorption spectroscopy (IRRAS) using CO as a probe molecule. The chemical activity of the formed ZnO films is probed by measuring the stretch frequency and binding energy of adsorbed CO.[25] We observe a different reactivity of the bilayer ZnO on Ag as evidenced by a much weaker CO adsorption and a blue shift of the CO vibrational frequency compared to ZnO/Cu. The results are interpreted in terms of the structure and electronic properties of ZnO/Ag by comparison to DFT calculations.

2. METHODS

2.1. Experimental Methods. The IRRAS and XPS measurements were performed in an IR/XPS ultrahigh vacuum (UHV) apparatus, which combines a state of the art FTIR spectrometer (Bruker Vertex 80v) with a multichamber UHV system (Prevac).[25] The AgZn(111) single crystal surface (Ag/Zn ratio 9:1) was cleaned by cycles of Ar$^+$ sputtering (1.5 kV, 10 mA, 1×10^{-6} mbar) at room temperature, followed by annealing at 420 K. Additionally, the cleanliness and oxidation states of the sample were monitored by XPS equipped with a VG Scienta R4000 electron energy analyzer. Exposure to CO at 65 K (cooling with liquid helium) was achieved by using a leak valve based directional doser connected to a tube (2 mm in diameter) that terminated 3 cm from the sample surface and 50 cm from the hot cathode ionization gauge. IR data were accumulated by recording typically 1024 scans with a resolution of 4 cm^{-1}. Prior to each exposure, a spectrum of a clean sample was recorded as a background reference.

The ZnO thin layers grown on the AgZn(111) substrate were prepared by oxidation of the clean AgZn(111) surface in O_2 atmosphere (1×10^{-5} mbar) at different temperatures for different periods of time. The thickness of the ZnO adlayers formed on the Ag substrate upon oxidation was determined based on the relative intensity of the Zn $2p_{3/2}$ and Ag $3d_{5/2}$ XPS signals using the following expression:[26]

$$\frac{I_A}{I_S} = \frac{T_A \sigma_A n_A \lambda_A(E_A)}{T_S \sigma_S n_S \lambda_S(E_S)} \cdot \frac{1 - e^{-d/\lambda_A(E_A)\cdot\cos(\theta)}}{e^{-d/\lambda_A(E_S)\cdot\cos(\theta)}}$$

Here, I_A and I_S denote the intensities of the adsorbate (Zn) and substrate (Ag) XPS signals at a grazing angle $\theta = 70°$, σ_A and σ_S refer to the photoionization cross sections for Zn $2p_{3/2}$ (18.92) and Ag $3d_{5/2}$ (10.66) (taken from ref 27). The mean free paths of the photoelectrons were calculated to amount to $\lambda_A(E_A) =$ 11.96 Å, $\lambda_A(E_S) = 27.28$ Å and $\lambda_S(E_S) = 15.2$ Å.[28,29] n_A and n_S denote the atomic density of ZnO and Ag species. For ZnO, two different structures were considered: wurzite -4.89×10^{-2} atoms/Å^3, graphitic -4.08×10^{-2} atoms/Å^3.[15,30] For Ag, $n_S =$ 5.89×10^{-2} atoms/Å^3.

The binding energy of CO adsorbed to different sites was estimated based on temperature dependent IR experiments. IR spectra were recorded continually while heating the sample with a constant rate of 0.05 K/s. The normalized peak areas were shown as a function of temperature. The activation energies (E_d) for desorption of CO from the different sites were estimated via the Redhead equation[31] assuming a pre exponential factor of 10^{13} s^{-1}.

2.2. Theoretical Methods. The calculations were performed with the full potential, all electron simulation package FHI aims.[32] Electronic exchange and correlation was treated using either the generalized gradient approximation (GGA) type Perdew−Burke−Ernzerhof (PBE) functional[33] or the screened hybrid functional HSE06[34,35] together with the Tkatchenko−Scheffler (TS) semiempirical correction scheme for dispersion interactions.[36] The TS parameters for Ag and ZnO were taken from ref 23 and account for surface and polarization effects.[37,38] The PBE and HSE06 optimized lattice constants for Ag, monolayer ZnO and bulk wurtzite ZnO were taken from ref 23 as well. *Tight* default settings were used for the basis set and integration grids. Test results using *really tight* settings for CO adsorption on the wurtzite (1010) surface showed that binding energies and frequencies were converged to within 1−2 meV and 1−2 cm^{-1}, respectively. The ZnO/Ag system was modeled using the experimentally observed coincidence structure corresponding to a (7 × 7) graphitic bilayer ZnO film on a (8 × 8) Ag(111) substrate[19] as in previous theoretical studies[24,39] and a four layered metal slab (PBE calculations). The size of the ZnO/Ag supercell was fixed by the PBE optimized lattice constant of Ag (4.15 Å) and the ZnO lattice constant was adjusted accordingly, resulting in a ∼ 2% tensile strain in ZnO compared to the PBE optimized lattice constant of a free standing monolayer ZnO sheet (3.28 Å). For the HSE06 calculations and due to the high computational cost of hybrid functional calculations, we instead modeled the ZnO/Ag system using a (2 × 2) graphitic bilayer ZnO film on a (2 × 2) Ag(111) substrate. In these calculations, we instead released the strain in the lateral directions on Ag, resulting in a tensile strain of ∼11%. The Ag slab contained two layers with an interlayer distance that had been relaxed to compensate for the strain in the lateral directions. The ZnO film was kept fixed in a flat geometry with interlayer distances corresponding to the mean distances obtained with PBE in the (7 × 7)ZnO/(8 × 8)Ag calculation. Bulk wurtzite ZnO with the (1010) surface termination was modeled using four ZnO

layers and a (2×1) cell. This cell contains four Zn atoms at two inequivalent heights in the top layer and is thus comparable in lateral size to a (2×2) cell for ZnO in the flat graphitic structure.

For the $(7 \times 7)ZnO/(8 \times 8)Ag$ calculation the Brillouin zone was sampled using a (2×2) k point grid. For the remaining smaller structures a (4×4) k point grid was used. Denser k point grids were used for the density of states calculations. A vacuum region of 30 Å perpendicular to the surface separated the slabs from their periodic images and a dipole correction was applied.[40] For the $(7 \times 7)ZnO/(8 \times 8)$ Ag and $ZnO(10\overline{1}0)$ calculations the two bottom layers were kept fixed in their bulk truncated positions, while the top layers and adsorbed CO were relaxed until the maximum force in the system fell below 0.01 eV/Å. For the $(2 \times 2)ZnO/(2 \times 2)Ag$ calculations, only the adsorbed CO molecule was relaxed. The (harmonic) vibrational frequency of the CO stretching mode was calculated using a finite difference scheme.

3. RESULTS AND DISCUSSION

3.1. XPS Data. The growth of thin ZnO adlayers was monitored by highly surface sensitive grazing emission XPS and Auger electron spectroscopy (AES). The XPS and AES data in Figure 1 and Figure S1 reveal that the clean AgZn(111) alloy
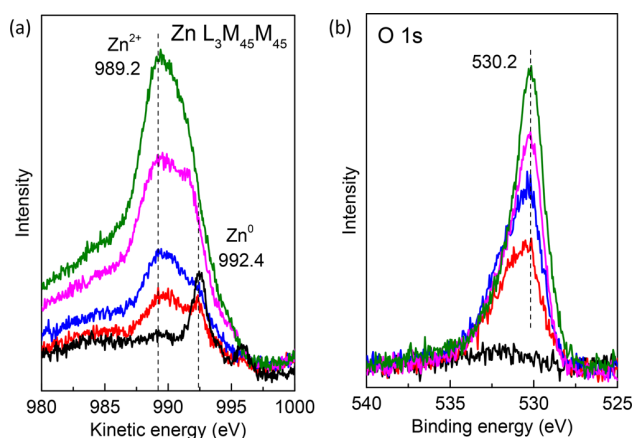
Figure 1. Grazing emission (a) Zn $L_3M_{45}M_{45}$ Auger spectra and (b) O 1s spectra recorded before (black curve) and after oxidation of the AgZn(111) sample with O_2 (1×10^{-5} mbar for 10 min) at 300 K (red curve), 420 K (blue curve), 500 K (magenta curve), and 600 K (olive curve).

surface is dominated by Ag species. The Zn $L_3M_{45}M_{45}$ Auger spectra are sensitive to the oxidation state of zinc and show large changes in the line shape with an energy difference of about 4 eV between Zn^{2+} and metallic Zn^0.[41,42] However, a clear chemical shift is not observed in the Zn 2p core level spectra (see Figures S2 and S3) due to screening effects in the final core−hole state.[42] The weak Zn $L_3M_{45}M_{45}$ Auger peak at 992.4 eV (kinetic energy, KE) demonstrates the presence of a very small portion of metallic Zn component ($\sim$2%) at the surface, which is substantially lower than the nominal concentration of Zn in the bulk (10%) of the sample. Exposure of the AgZn(111) substrate to molecular oxygen at room temperature leads to the formation of surface ZnO species, as confirmed by the appearance of the typical Zn^{2+} $L_3M_{45}M_{45}$ peak at 989.2 eV (KE) and the O 1s peak at 530.2 eV. Note that the oxidized zinc species is characterized by a much broader and

asymmetric (at the higher BE side) line shape as compared to metallic Zn.[41] Upon further oxidation at elevated temperatures, the Zn^{2+} and O^{2-} related XPS signals increase gradually in intensity, indicating a pronounced increase of the surface Zn concentration (Figure 1).

On the basis of a quantitative analysis of the intensity ratio between Zn $2p_{3/2}$ and Ag $3d_{5/2}$ XPS data (Figures S2 and S3), the average thickness of the thin ZnO adlayer can be estimated. This yields a value of about 1.9 Å (assuming graphitic type ZnO) after oxidation of the AgZn substrate with O_2 (1×10^{-5} mbar) at 600 K for 10 min, corresponding to the presence of 1 ML of ZnO. Prolonged oxidation for 20 min leads to the formation of a ZnO bilayer (3.4 Å for planar ZnO). Exposure of the sample to O_2 at 600 K for 40 min results in a further growth of ZnO films with an average thickness of about 4.4 Å (assuming graphitic type ZnO) or 3.7 Å (assuming wurtzite type ZnO).

3.2. IRRAS Data. Pristine and oxidized AgZn(111) surfaces were further characterized by IRRAS using CO as a probe molecule (see Figure 2). After CO adsorption on the oxygen
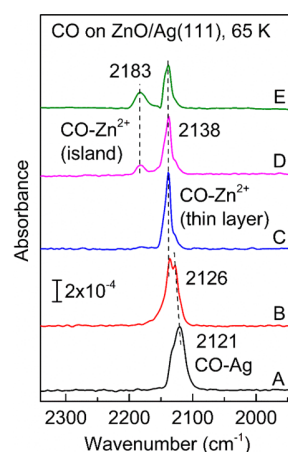
Figure 2. IRRAS data recorded after 1 L CO adsorption on the pristine and oxidized AgZn(111) surfaces at 65 K. The ZnO adlayers were prepared by oxidizing the (A) AgZn(111) surface in 1×10^{-5} mbar O_2 atmosphere at 500 K for (B) 10 min, and at 600 K for (C) 10 min, (D) 20 min, (E) 40 min.

free AgZn(111) surface at 65 K, a predominant IR band was observed at 2121 cm^{-1} (see Figure 2A), which is assigned to CO bound to Ag sites. This band disappears upon slightly heating to 70 K, indicating a rather weak interaction between CO and Ag. This finding is in good agreement with the results of CO adsorption on Ag(111) reported by Jacobi and co workers.[43] They found that CO is weakly bound to Ag sites (physisorption) with a random orientation of the molecular axis in the monolayer.

Oxidation at 500 K leads to the appearance of a second IR band at 2136 cm^{-1} (Figure 2B), while the intensity of the Ag bonded CO band decreases, accompanied by a slight blue shift to 2126 cm^{-1}. After further exposure to oxygen at 600 K for 10 min, only one single, sharp CO peak at 2138 cm^{-1} is detected, whereas the Ag related IR band disappears completely (Figure 2C). Our IRRAS data, together with the XPS/AES results discussed in section 3.1, provide solid evidence for the formation of a closed monolayer of ZnO after this oxidation treatment. Furthermore, the IR spectrum remains nearly unchanged for ZnO films with a thickness of 0.34 nm

(corresponding to a ZnO bilayer, see Figure 2D). Therefore, we conclude that the 2138 cm^{-1} band is characteristic for CO species adsorbed to Zn^{2+} sites on the surface of ZnO thin layers. It should be noted that other approaches (e.g., Zn deposition in oxygen atmosphere) typically result in not closed ZnO thin films.

More extended oxidation at 600 K for prolonged time leads to the appearance of a weak high frequency CO vibration at 2183 cm^{-1}, which becomes more pronounced at ZnO coverages higher than 2 ML (see Figure 2E). Simultaneously, the 2138 cm^{-1} band decreases in intensity. These observations suggest the coexistence of a thin ZnO bilayer and thicker ZnO clusters (islands). The IR band at 2183 cm^{-1} is in good agreement in frequency with those reported for CO adsorption on ZnO single crystal surfaces.[44−46] The substantial blue shift (40 cm^{-1}) compared to the gas phase value indicates that the interaction between CO and the thicker ZnO islands is dominated by the electrostatic interaction (Stark effect and Pauli repulsion)[47] and possibly electron donation from the CO 5σ orbital to the surface Zn cations (see also theoretical analysis in Sect. 3.4), in accord with CO adsorption on wurtzite type ZnO substrates.[25] These findings reveal that wurtzite type ZnO islands are formed for thickness above 2 ML on Ag(111), in line with the STM and SXRD observations.[19]

The temperature dependent IRRAS experiments (see Figure 3) provide insight into the thermal stability of various CO
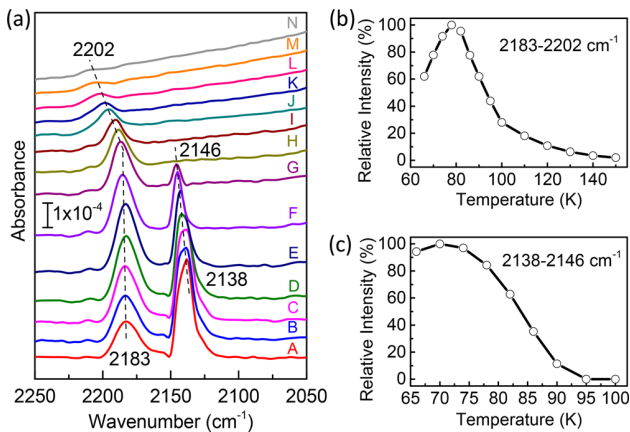
Figure 3. (a) IRRAS spectra recorded after exposing the thin ZnO adlayers to 1 L CO at (A) 66 K and then heating gradually to higher temperatures: (B) 70 K, (C) 74 K, (D) 78 K, (E) 82 K, (F) 86 K, (G) 90 K, (H) 95 K, (I) 100 K, (J) 110 K, (K) 120 K, (L) 130 K, (M) 140 K, (N) 150 K. (b) Normalized intensity of the high frequency band as a function of sample temperature. (c) Normalized intensity of the low frequency band as a function of sample temperature.

species. Interestingly, the intensity of both CO bands increases first upon heating to about 75 K. This is attributed to a restructuring process of the CO adlayer from a nonuniform, disordered distribution at low temperatures (66 K) to a more ordered structure, as observed for CO adsorption on ceria surfaces.[48] Further raising the temperature leads to a gradual attenuation of both CO signals due to thermal induced desorption. Based on a quantitative analysis of the IR data (see Figure 3b,c) and assuming a pre exponential factor of 10^{13} s^{-1}, the binding energies were determined to amount to 0.30 eV (29 kJ/mol) for CO adsorbed to wurtzite type ZnO clusters (islands) and 0.24 eV (23 kJ/mol) for ZnO bilayer bonded CO species, respectively. The binding energy of 0.30 eV is

consistent with those determined for CO bound to Zn^{2+} sites on ZnO(1010) (0.32 eV) and Zn ZnO(0001) (0.28 eV) surfaces.[44−46] These results reveal that CO is more weakly bound to bilayer ZnO formed on Ag(111) compared to thicker wurtzite type ZnO islands, which is in contrast to the observation of a significantly enhanced interaction of CO with ultrathin ZnO films on Cu(111).[10] The present IRRAS data provide direct evidence that the metal substrate plays a crucial role in the chemical properties of the ultrathin ZnO films.

Importantly, we found a clear blue shift for both CO species with annealing to higher temperatures (see Figure 3a), i.e., with decreasing CO coverage. At very low coverage ($\theta \rightarrow 0$, isolated CO adsorbates), the IR bands are located at 2146 cm^{-1} for CO adsorbed on the ZnO bilayer surface and at 2202 cm^{-1} for CO on wurtzite type ZnO islands. This coverage induced frequency shift is attributed to lateral adsorbate−adsorbate interactions including both dynamic (dipole−dipole coupling) and substrate mediated static effects (for details, please see refs 25 and 44).

3.3. DFT Results. To support the assignment of the IRRAS bands, we carried out DFT calculations of CO adsorption energies and vibrational frequencies. The use of GGA type DFT functionals for adsorption on ZnO is in general not uncritical due to the well known issues with describing the electronic structure of oxides at the GGA level of theory. A hybrid functional like the HSE06, on the other hand, can generally be expected to perform better, since it improves on the self interaction error in DFT by incorporating a portion of Hartree−Fock exact exchange. To illustrate this we compare data for CO adsorption on the wurtzite (1010) surface obtained at the PBE and HSE06 levels of theory (see Table 1). The CO molecule adsorbs to a Zn atom in a tilted geometry, which is rotated about 25 degrees from the surface normal (see Figure 4a). While both functionals give very similar values for the structural data (tilt angle, binding distance) and the adsorption energy (0.45 eV with PBE and 0.47 eV with HSE06) in reasonable agreement with available experimental measurements (0.32 eV[46]), the vibrational frequencies come out very different. The HSE06 functional correctly reproduces the blue shift of around 40 cm^{-1} with respect to the gas phase frequency that is found experimentally,[44] while the PBE functional gives a shift around zero. A similar improvement of performance as regards vibrational shifts by using a hybrid functional (PBE0) was recently reported by Tosoni et al.[39]

As mentioned in the previous section, we expect that the high frequency band shifted around 40 cm^{-1} with respect to the gas phase, which is measured after prolonged oxidation, results from CO adsorbed to thick ZnO films. A recent DFT study on the structure of ZnO islands in the 3−4 ML range on top of the closed 2 ML film suggested that such islands will undergo a structural transition to a wurtzite like phase.[24] The present HSE06 result of a shift of around 40 cm^{-1} for the wurtzite structure is therefore in excellent agreement with the measured high frequency band at 2183 cm^{-1} observed after the saturation of CO adsorption (curve A in Figure 3a). Due to the high computational cost of hybrid functional calculations, the present result was calculated for a rather high CO coverage of 0.5 ML. However, as discussed in ref 39, the shift (both at the GGA and hybrid functional level) tends to become more positive for lower coverages. This effect is in good agreement with the shift to higher frequencies observed after annealing, i.e., gradually decreasing CO coverage (curves E−N in Figure 3a).

Table 1. Calculated and Experimental CO Adsorption Energies E_{CO} (in eV), Zn−C Binding Distances d_{Zn-C} (in Å), Tilt of the CO Molecule with Respect to the Surface Normal α (in deg.), Shift of the C−O Binding Distance with Respect to the Gas Phase Value (1.135 Å with PBE and 1.122 Å with HSE06) Δd_{C-O} (in Å), and Shift of the CO Vibrational Frequency with Respect to the Gas Phase Value (2128 cm^{-1} with PBE and 2238 cm^{-1} with HSE06) Δv_{CO} (in cm^{-1})

system	method	E_{CO}	d_{Zn-C}	α	Δd_{C-O}	Δv_{CO}
ZnO(10$\bar{1}$0)	PBE+TS	0.45	2.19	25	0.001	+7
	HSE06+TS	0.47	2.23	28	0.004	+37
	PBE+U+D2$'^{b}$		2.16	40	~0	5
	PBE0+D2^{a,b}	0.57	2.13	35	0.004	+41
	exp.	0.32^{c}				+42^{d}
(7 × 7)ZnO/(8 × 8)Ag	PBE+TS: Site I	0.36	2.27	38	0.002	+5
	PBE+TS: Site II	0.24	2.33	41	0.001	3
	PBE+U+D2$'^{b}$	0.24	2.24	9	0.003	+6
	exp.	0.24				+3
(2 × 2)ZnO/(2 × 2)Ag	PBE+TS	0.13	2.85	61	+0.001	16
	HSE06+TS	0.12	2.88	56	~0	5

^{a}Obtained in a (3 × 2) cell using eight ZnO layers. ^{b}From ref 39. ^{c}From ref 46. ^{d}From ref 44.
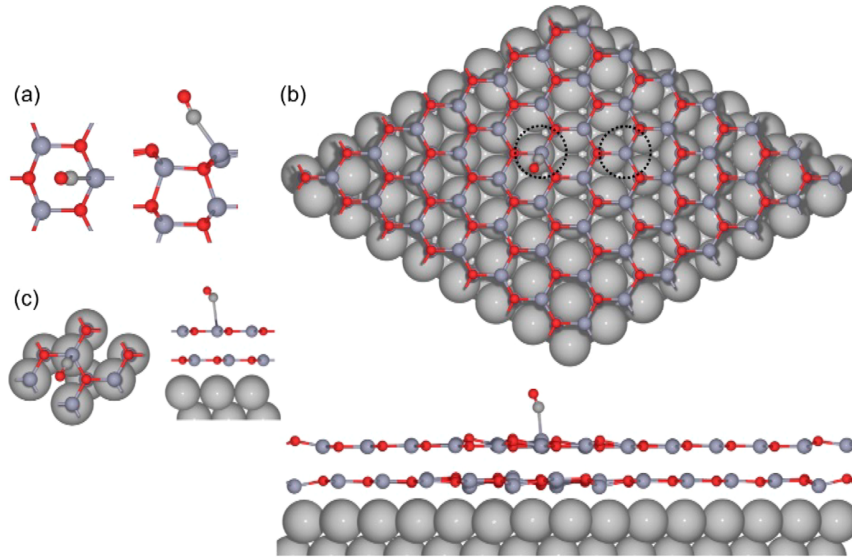

Figure 4. DFT optimized structures (top and side view) of CO adsorbed on (a) the wurtzite (1010) surface, (b) the large (7 × 7)ZnO/(8 × 8)Ag structure and (c) the smaller (2 × 2)ZnO/(2 × 2)Ag structure. For clarity, the bonds between the flat graphitic ZnO layers have been omitted. In panel b, the dashed black circles highlight adsorption site I (shown structure) and II (empty circle).

Before analyzing further the problematic description of CO adsorption on ZnO at the GGA level, we present also the results for the bilayer ZnO/Ag system. In Table 1 we report PBE data for two different adsorption sites I and II within the Moiré supercell of the full (7 × 7)ZnO/(8 × 8)Ag structure (see Figure 4b). At site I CO binds the strongest with 0.36 eV, whereas at site II the binding is reduced to 0.24 eV. Given that CO is dosed at very low temperatures in the present experimental work, we expect several site types within the Moiré supercell to be populated. The derived experimental binding energy of 0.24 eV corresponds then rather well with the calculated values, assuming that the experiment likely measures the average binding energy for several different sites. The CO binding energy on ZnO/Ag is thus much lower than the binding energy obtained at the wurtzite surface in the present work (0.45 eV using PBE) and the previously reported binding energy of 0.52 eV for ZnO/Cu (also PBE),[10] indicating that the CO molecule is only bound by weak dispersive interactions on ZnO/Ag. This different behavior is attributed to the flat geometry of the ZnO bilayer adsorbed on an Ag(111)

surface (see Figure 4b) as compared to the buckled structure of ZnO in the wurtzite structure (see Figure 4a) and the previously identified rumpling of the ZnO bilayer on a Cu(111) surface.[10] For the vibrational frequency, we obtain a slight blue shift of 5 cm^{-1} (site I) and a slight red shift of 3 cm^{-1} (site II) for ZnO/Ag using PBE. These values correspond well with the measured low frequency band at low coverage (see curve G in Figure 3a), which is blue shifted by 3 cm^{-1} with respect to gas phase CO. Our results are also in good agreement with recent results reported by Tosoni et al. (0.24 eV binding energy, frequency blue shifted by 6 cm^{-1}).[39]

The question that remains, in light of the above described failure of PBE to describe the frequency shift for the wurtzite (1010) surface, is whether the good agreement with experiment obtained at the PBE level of theory for the ZnO/Ag system is real or results from a fortuitous cancellation of errors. To answer this question, we proceed to a direct comparison of PBE and HSE06 for the ZnO/Ag system. Due to the high computational cost of hybrid functional calculations, we are presently not able to consider the full (7 × 7)ZnO/(8 × 8)Ag
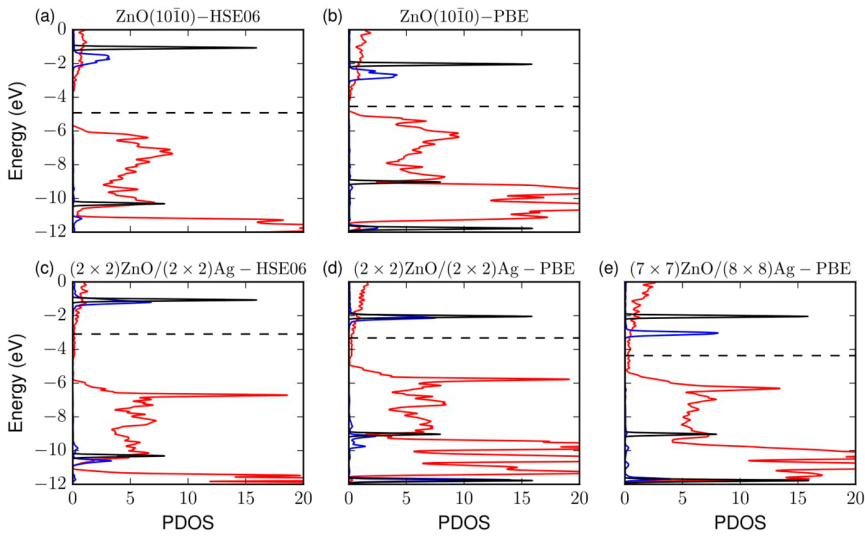
Figure 5. DFT projected density of states (PDOS) for CO adsorbed to various surfaces calculated using either PBE or HSE06. Red curves are projected onto ZnO, blue curves are projected onto the CO molecule, and the levels of the isolated CO molecule are superimposed in black. The Fermi level is marked with a dashed line. (a) ZnO(10$\bar{1}$0) HSE06, (b) ZnO(10$\bar{1}$0) PBE, (c) (2 × 2)ZnO/(2 × 2)Ag HSE06, (d) (2 × 2)ZnO/(2 × 2)Ag PBE, and (e) (7 × 7)ZnO/(8 × 8)Ag PBE.

structure at the HSE06 level of theory. Instead, we consider a smaller (2 × 2)ZnO/(2 × 2)Ag structure where the residual strain is released on the Ag and the bilayer ZnO film is kept fixed in a flat geometry as described in Section 2.2 (see Figure 4c). The CO adsorption energies calculated with PBE and HSE06 for this structure are around 0.13 eV (see Table 1). The reduced binding, which is also reflected in the enlarged Zn−C binding distance of around 2.8 Å (as compared to around 2.2 Å for the other systems considered), is likely a consequence of the fixed, flat geometry of the ZnO film. Interestingly, the vibrational frequencies also come out very similar at the PBE and HSE06 levels of theory, with the PBE frequency being only slightly (~10 cm^{-1}) more red shifted than the HSE06 frequency. Comparing on the other hand the frequencies calculated with PBE for the large and small ZnO/Ag supercells, it is seen that the small system is ~20 cm^{-1} more red shifted than the large system. The difference between the large and the small supercells should be mainly of electrostatic origin resulting from the difference in work function of the strained two layer versus unstrained four layer Ag slabs, the slightly larger buckling of ZnO in the large supercell and the enlarged distance of the CO from the surface in the small supercell. Assuming that the effect of these changes is well described using PBE, we can estimate a hybrid vibrational shift for the large supercell by adding the difference between the HSE06 and PBE frequencies for the small supercell (~10 cm^{-1}) to the PBE shift for the large supercell, resulting in an effective HSE06 blue shift of ~10 cm^{-1}. This value is still consistent with the experimental measurement. Therefore, based on the good agreement between PBE and HSE06 for the small ZnO/Ag supercell and the similarity of the small and large supercells, we expect that the good agreement with experiment obtained with PBE for the large supercell is trustworthy.

3.4. Analysis and Discussion of DFT Results. As discussed in ref 25, the vibrational frequency shift of CO on ZnO surfaces is generally explained via two mechanisms: (i) the electrostatic interaction with the electric field of the surface metal cations (Stark effect) and (ii) electron donation and back donation to the CO frontier orbitals (Blyholder model[49]).

The former effect polarizes the CO molecule and strengthens the internal bond, which leads to a shortening of the bond and a blue shifted frequency. The latter effect can lead to either a blue shift in case electrons are donated from the 5σ highest occupied molecular orbital (HOMO) to the surface or a red shift in case electrons are back donated from the surface into the 2π* lowest unoccupied molecular orbital (LUMO).

In order to further investigate which of these mechanisms are at play in the various systems, we plot in Figure 5 the projected density of states onto ZnO (red curves) and onto the CO molecule (blue curves). The levels of the isolated CO molecule are in each case superimposed in black. We begin by comparing CO on ZnO(10$\bar{1}$0) calculated with HSE06 (Figure 5a) and PBE (Figure 5b). As expected, the use of a hybrid functional (HSE06) corrects for the GGA level underestimation of the ZnO band gap and HOMO−LUMO gap of the isolated CO molecule. The Fermi level is influenced by the position of the valence band maximum (VBM) and therefore shifts from −4.55 eV with PBE to −4.92 eV with HSE06 relative to the vacuum level. This increase in the work function for HSE06 leads to a larger electric field at the surface, which is expected to give a larger blue shift of the CO vibrational frequency. Considering now the HOMO and LUMO levels, we note that the interaction of the CO molecule with the surface leads to a significant down shift and broadening of the LUMO level, which brings it close to the Fermi level. In that context it is worth noting that the observed tilted adsorption geometry of the CO molecule favors the hybridization of the LUMO level with the surface states since it is of π symmetry. The HOMO level also shows a large degree of hybridization; however, since it is located rather far away from the Fermi level, we expect that back donation into the LUMO level will play the largest role in the Blyholder model. Using PBE, we calculate a vibrational shift close to zero. We therefore tentatively suggest that the two opposite effects are at play, blue shift from the Stark effect and red shift from back donation into the 2π* orbital, largely cancel each other. With the HSE06 functional, on the other hand, we expect the blue shift to dominate as a consequence of the increased work function and the increased distance between the

LUMO level and the Fermi level. Indeed, only the HSE06 functional is observed to correctly reproduce the 40 cm^{-1} blue shift observed experimentally.

Next, we turn to the comparison of HSE06 and PBE for the (2×2)ZnO/(2×2)Ag structure. As for the ZnO($10\overline{1}0$) surface, we observe a larger ZnO band gap with the hybrid functional. However, as a consequence of n type doping from the metal surface, the Fermi level now moves up in the conduction band and both functionals give a very similar (reduced) value for the work function (3.32 eV with PBE and 3.10 eV with HSE06). We therefore expect also a similar blue shift from the Stark effect for the two functionals. Compared to ZnO($10\overline{1}0$), it is seen that the LUMO level interacts much less with the surface for (2×2)ZnO/(2×2)Ag, which is related to the much weaker binding of CO to ZnO/Ag in general and to ZnO/Ag in the smaller, constrained structure in particular (as evidenced by the lower binding energies and enlarged binding distances, see Table 1). The amount of red shifting of the CO vibrational frequency is expected to be dependent both on how close the LUMO level is to the Fermi level and how strongly it hybridizes. For HSE06, the LUMO level is located slightly further away from the Fermi level and we therefore expect the HSE06 frequency to be blue shifted with respect to PBE, which is indeed the case (by ~10 cm^{-1}). The rather small difference between the HSE06 and PBE results is likely a consequence of the very small degree of hybridization in this system.

Finally, we compare the (7×7)ZnO/(8×8)Ag (site I) and (2×2)ZnO/(2×2)Ag structures at the PBE level of theory. It is seen that the degree of hybridization of the LUMO level and its distance to the Fermi level are very similar in the two systems. The most notable change is a decrease in the work function to 3.32 eV for the (2×2)ZnO/(2×2)Ag structure compared to 4.37 eV for the (7×7)ZnO/(8×8)Ag system, which likely derives from the fixed geometry of the ZnO film and the strain in the Ag slab in the former system. As a consequence, we would expect the CO frequency to be more blue shifted in the (7×7)ZnO/(8×8)Ag system, which is indeed the case (by ~20 cm^{-1}).

Compared to the present ZnO/Ag system, the ZnO bilayer on Cu(111) reported in ref 10 exhibits a much more pronounced buckling. We suggest that the much stronger interaction of CO with this buckled film (a binding energy of 0.54 eV was found for ZnO/Cu in ref 10 as compared to the binding energy of 0.24 eV found for ZnO/Ag in the present work) leads to a stronger back donation and an overall more red shifted CO frequency than in the present system. We note that a recent study by Tosoni et al. reported a red shift in the ZnO/Cu system of similar magnitude as found experimentally for a film geometry that was flattened by artificial strain in the chosen supercell setup.[39] Their computed binding energy largely underestimated the experimentally determined binding though. Tentatively, we therefore ascribe the agreement of their calculated frequency with experiment to a fortuitous under estimation of both the blue shifting Stark effect and the hybridization induced red shift.

4. CONCLUSIONS

As demonstrated by our experimental and theoretical results, the metal support plays a crucial role in the chemical activity of thin ZnO adlayers. The previously reported red shift by about 70 cm^{-1} for CO on ZnO/Cu relative to the normal stretch frequency for CO on wurtzite surfaces is substantially modified when changing the metal substrate. In the ZnO/Ag system we find a frequency similar to the gas phase CO vibrational frequency (red shifted by around 40 cm^{-1} with respect to wurtzite) for CO adsorbed on flat bilayer ZnO films and a frequency similar to previous results for wurtzite surfaces for CO adsorbed on thicker ZnO islands in the 3−4 ML range. Whereas on Cu the ZnO film has been reported to buckle substantially, we find that it adopts a flat graphitic like structure on Ag. This difference, which is driven by the different lattice constants of the two metals (3.61 Å (Cu) vs 4.09 Å (Ag)), has pronounced consequences for the adsorption energy of CO, which is much decreased in the presence of an Ag substrate as compared to a Cu substrate. Our results thus illustrate the variety of ZnO phases that can be formed and the pronounced influence of the metal substrate for ultrathin ZnO films.

From the theoretical side, we have shown that GGA type DFT functionals cannot uncritically be applied to the study of CO adsorption on ZnO. This is especially problematic for the wurtzite ZnO($10\overline{1}0$) surface, where the incorrect level alignment results in a severe underestimation of the blue shift of the CO stretch frequency. CO binding energies, on the other hand, come out very similar at the hybrid and GGA levels. For ZnO/Ag, the frequencies seem to be much less sensitive to the errors in the level alignment, and good agreement with experiment is already obtained at the GGA level. Our analysis ascribes this difference to two effects: In contrast to the wurtzite ZnO($10\overline{1}0$) surface, the work function is pinned by the metallic Fermi level, which is similarly described by both GGA and hybrid functionals. While this leads to a similar Stark contribution to the frequency shift, the hybridization with the surface is much weaker at the less corrugated ZnO/Ag film. Functional errors in the frontier level positions are therefore less consequential, as the resulting different donation and back donation contributions to the overall frequency shift are smaller.

■ AUTHOR INFORMATION

Corresponding Authors
*E mail: mie.andersen@ch.tum.de (M.A.).
*E mail: yuemin.wang@kit.edu (Y.W.).

Mie Andersen: 0000 0002 9943 1534
Yuemin Wang: 0000 0002 9963 5473
Christof Wöll: 0000 0003 1078 3304
Karsten Reuter: 0000 0001 8473 8659
Author Contributions
§M.A. and X.Y. contributed equally to this work.
Notes
The authors declare no competing financial interest.

■ REFERENCES

(1) Freund, H. J.; Pacchioni, G. Oxide Ultra Thin Films on Metals: New Materials for the Design of Supported Metal Catalysts. *Chem. Soc. Rev.* **2008**, *37*, 2224−2242.

(2) Naumann d'Alnoncourt, R.; Xia, X.; Strunk, J.; Loffler, E.; Hinrichsen, O.; Muhler, M. The Influence of Strongly Reducing Conditions on Strong Metal−Support Interactions in Cu/ZnO Catalysts Used for Methanol Synthesis. *Phys. Chem. Chem. Phys.* **2006**, *8*, 1525−1538.

(3) Sun, Y. N.; Giordano, L.; Goniakowski, J.; Lewandowski, M.; Qin, Z. H.; Noguera, C.; Shaikhutdinov, S.; Pacchioni, G.; Freund, H. J. The Interplay between Structure and CO Oxidation Catalysis on Metal Supported Ultrathin Oxide Films. *Angew. Chem., Int. Ed.* **2010**, *49*, 4418−4421.

(4) Sonström, P.; Arndt, D.; Wang, X.; Zielasek, V.; Bäumer, M. Ligand Capping of Colloidally Synthesized Nanoparticles−A Way to Tune Metal−Support Interactions in Heterogeneous Gas Phase Catalysis. *Angew. Chem., Int. Ed.* **2011**, *50*, 3888−3891.

(5) Naumann d'Alnoncourt, R.; Friedrich, M.; Kunkes, E.; Rosenthal, D.; Girgsdies, F.; Zhang, B.; Shao, L.; Schuster, M.; Behrens, M.; Schlögl, R. Strong Metal−Support Interactions between Palladium and Iron Oxide and Their Effect on CO Oxidation. *J. Catal.* **2014**, *317*, 220−228.

(6) Willinger, M. G.; Zhang, W.; Bondarchuk, O.; Shaikhutdinov, S.; Freund, H. J.; Schlögl, R. A Case of Strong Metal−Support Interactions: Combining Advanced Microscopy and Model Systems to Elucidate the Atomic Structure of Interfaces. *Angew. Chem., Int. Ed.* **2014**, *53*, 5998−6001.

(7) Tauster, S. J. Strong Metal Support Interactions. *Acc. Chem. Res.* **1987**, *20*, 389−394.

(8) Kattel, S.; Ramírez, P. J.; Chen, J. G.; Rodriguez, J. A.; Liu, P. Active Sites for CO_2 Hydrogenation to Methanol on Cu/ZnO Catalysts. *Science* **2017**, *355*, 1296−1299.

(9) Lunkenbein, T.; Schumann, J.; Behrens, M.; Schlögl, R.; Willinger, M. G. Formation of a ZnO Overlayer in Industrial Cu/ZnO/Al_2O_3 Catalysts Induced by Strong Metal−Support Interactions. *Angew. Chem., Int. Ed.* **2015**, *54*, 4544−4548.

(10) Schott, V.; Oberhofer, H.; Birkner, A.; Xu, M.; Wang, Y.; Muhler, M.; Reuter, K.; Wöll, C. Chemical Activity of Thin Oxide Layers: Strong Interactions with the Support Yield a New Thin Film Phase of ZnO. *Angew. Chem., Int. Ed.* **2013**, *52*, 11925−11929.

(11) Schumann, J.; Kröhnert, J.; Frei, E.; Schlögl, R.; Trunschke, A. IR Spectroscopic Study on the Interface of Cu Based Methanol Synthesis Catalysts: Evidence for the Formation of a ZnO Overlayer. *Top. Catal.* **2017**, *60*, 1735−1743.

(12) Martynova, Y.; Liu, B. H.; McBriarty, M. E.; Groot, I. M. N.; Bedzyk, M. J.; Shaikhutdinov, S.; Freund, H. J. CO Oxidation over ZnO Films on Pt(111) at near Atmospheric Pressures. *J. Catal.* **2013**, *301*, 227−232.

(13) Pan, Q.; Liu, B. H.; McBriarty, M. E.; Martynova, Y.; Groot, I. M. N.; Wang, S.; Bedzyk, M. J.; Shaikhutdinov, S.; Freund, H. J. Reactivity of Ultra Thin ZnO Films Supported by Ag(111) and Cu(111): A Comparison to ZnO/Pt(111). *Catal. Lett.* **2014**, *144*, 648−655.

(14) Naumann d'Alnoncourt, R.; Kurtz, M.; Wilmer, H.; Loffler, E.; Hagen, V.; Shen, J. Y.; Muhler, M. The Influence of ZnO on the Differential Heat of Adsorption of CO on Cu Catalysts: A Microcalorimetric Study. *J. Catal.* **2003**, *220*, 249−253.

(15) Freeman, C. L.; Claeyssens, F.; Allan, N. L.; Harding, J. H. Graphitic Nanofilms as Precursors to Wurtzite Films. *Phys. Rev. Lett.* **2006**, *96*, 066102.

(16) Liu, B. H.; Groot, I. M.N.; Pan, Q.; Shaikhutdinov, S.; Freund, H. J. Ultrathin Zn and ZnO Films on Cu(111) as Model Catalysts. *Appl. Catal., A* **2017**, *548*, 16−23.

(17) Kourouklis, H. N.; Nix, R. M. The Growth and Structure of ZnOx Overlayers on Low Index Silver Surfaces. *Surf. Sci.* **1994**, *318*, 104−114.

(18) Shiotari, A.; Liu, B. H.; Jaekel, S.; Grill, L.; Shaikhutdinov, S.; Freund, H. J.; Wolf, M.; Kumagai, T. Local Characterization of Ultrathin ZnO Layers on Ag(111) by Scanning Tunneling Microscopy and Atomic Force Microscopy. *J. Phys. Chem. C* **2014**, *118*, 27428−27435.

(19) Tusche, C.; Meyerheim, H. L.; Kirschner, J. Observation of Depolarized ZnO(0001) Monolayers: Formation of Unreconstructed Planar Sheets. *Phys. Rev. Lett.* **2007**, *99*, 026102.

(20) Deng, X.; Yao, K.; Sun, K.; Li, W. X.; Lee, J.; Matranga, C. Growth of Single and Bilayer ZnO on Au(111) and Interaction with Copper. *J. Phys. Chem. C* **2013**, *117*, 11211−11218.

(21) Stavale, F.; Pascua, L.; Nilius, N.; Freund, H. J. Morphology and Luminescence of ZnO Films Grown on a Au(111) Support. *J. Phys. Chem. C* **2013**, *117*, 10552−10557.

(22) Weirum, G.; Barcaro, G.; Fortunelli, A.; Weber, F.; Schennach, R.; Surnev, S.; Netzer, F. P. Growth and Surface Structure of Zinc Oxide Layers on a Pd(111) Surface. *J. Phys. Chem. C* **2010**, *114*, 15432−15439.

(23) Bieniek, B.; Hofmann, O. T.; Rinke, P. Influence of Hydrogen on the Structure and Stability of Ultra Thin ZnO on Metal Substrates. *Appl. Phys. Lett.* **2015**, *106*, 131602.

(24) Demiroglu, I.; Bromley, S. T. Evidence for Multi Polymorphic Islands During Epitaxial Growth of ZnO on Ag(111). *J. Phys.: Condens. Matter* **2016**, *28*, 224007.

(25) Wang, Y.; Wöll, C. IR Spectroscopic Investigations of Chemical and Photochemical Reactions on Metal Oxides: Bridging the Materials Gap. *Chem. Soc. Rev.* **2017**, *46*, 1875−1932.

(26) Merzlikin, S. V.; Tolkachev, N. N.; Strunskus, T.; Witte, G.; Glogowski, T.; Wöll, C.; Grünert, W. Resolving the Depth Coordinate in Photoelectron Spectroscopy − Comparison of Excitation Energy Variation Vs. Angular Resolved XPS for the Analysis of a Self Assembled Monolayer Model System. *Surf. Sci.* **2008**, *602*, 755−767.

(27) Scofield, J. H. Hartree Slater Subshell Photoionization Cross Sections at 1254 and 1487 eV. *J. Electron Spectrosc. Relat. Phenom.* **1976**, *8*, 129−137.

(28) Akkerman, A.; Boutboul, T.; Breskin, A.; Chechik, R.; Gibrekhterman, A.; Lifshitz, Y. Inelastic Electron Interactions in the Energy Range 50 eV to 10 keV in Insulators: Alkali Halides and Metal Oxides. Phys. *Phys. Status Solidi B* **1996**, *198*, 769−784.

(29) Tanuma, S.; Powell, C. J.; Penn, D. R. Calculations of Electron Inelastic Mean Free Paths. V. Data for 14 Organic Compounds over the 50−2000 eV Range. *Surf. Interface Anal.* **1994**, *21*, 165−176.

(30) Claeyssens, F.; Freeman, C. L.; Allan, N. L.; Sun, Y.; Ashfold, M. N. R.; Harding, J. H. Growth of ZnO Thin Films Experiment and Theory. *J. Mater. Chem.* **2005**, *15*, 139−148.

(31) Redhead, P. A. Thermal Desorption of Gases. *Vacuum* **1962**, *12*, 203−211.

(32) Blum, V.; Gehrke, R.; Hanke, F.; Havu, P.; Havu, V.; Ren, X.; Reuter, K.; Scheffler, M. Ab Initio Molecular Simulations with Numeric Atom Centered Orbitals. *Comput. Phys. Commun.* **2009**, *180*, 2175−2196.

(33) Perdew, J. P.; Burke, K.; Ernzerhof, M. Generalized Gradient Approximation Made Simple. *Phys. Rev. Lett.* **1996**, *77*, 3865−3868.

(34) Heyd, J.; Scuseria, G. E.; Ernzerhof, M. Hybrid Functionals Based on a Screened Coulomb Potential. *J. Chem. Phys.* **2003**, *118*, 8207−8215.

(35) Krukau, A. V.; Vydrov, O. A.; Izmaylov, A. F.; Scuseria, G. E. Influence of the Exchange Screening Parameter on the Performance of Screened Hybrid Functionals. *J. Chem. Phys.* **2006**, *125*, 224106.

(36) Tkatchenko, A.; Scheffler, M. Accurate Molecular Van der Waals Interactions from Ground State Electron Density and Free Atom Reference Data. *Phys. Rev. Lett.* **2009**, *102*, 073005.

(37) Ruiz, V. G.; Liu, W.; Zojer, E.; Scheffler, M.; Tkatchenko, A. Density Functional Theory with Screened Van Der Waals Interactions for the Modeling of Hybrid Inorganic Organic Systems. *Phys. Rev. Lett.* **2012**, *108*, 146103.

(38) Zhang, G. X.; Tkatchenko, A.; Paier, J.; Appel, H.; Scheffler, M. Van Der Waals Interactions in Ionic and Semiconductor Solids. *Phys. Rev. Lett.* **2011**, *107*, 245501.

(39) Tosoni, S.; Li, C.; Schlexer, P.; Pacchioni, G. CO Adsorption on Graphite Like ZnO Bilayers Supported on Cu(111), Ag(111), and Au(111) Surfaces. *J. Phys. Chem. C* **2017**, *121*, 27453−27461.

(40) Bengtsson, L. Dipole Correction for Surface Supercell Calculations. *Phys. Rev. B: Condens. Matter Mater. Phys.* **1999**, *59*, 12301−12304.

(41) Fox, J. H.; Nuttall, J. D.; Gallon, T. E. Solid State Effects in the Auger Spectrum of Zinc and Oxidised Zinc. *Surf. Sci.* **1977**, *63*, 390−402.

(42) Carley, A. F.; Roberts, M. W. Evidence for the Instability of Surface Oxygen at the Zn(0001) O Cu Interface from Core Level and X ray Induced Auger Spectroscopies. *Top. Catal.* **1996**, *3*, 91−102.

(43) Hansen, W.; Bertolo, M.; Jacobi, K. Physisorption of CO on Ag(111): Investigation of the Monolayer and the Multilayer through HREELS, ARUPS, and TDS. *Surf. Sci.* **1991**, *253*, 1−12.

(44) Buchholz, M.; Yu, X.; Yang, C.; Heißler, S.; Nefedov, A.; Wang, Y.; Wöll, C. IR Spectroscopy of CO Adsorption on Mixed Terminated ZnO Surfaces. *Surf. Sci.* **2016**, *652*, 247−252.

(45) Wang, Y.; Xia, X.; Urban, A.; Qiu, H.; Strunk, J.; Meyer, B.; Muhler, M.; Wöll, C. Tuning the Reactivity of Oxide Surfaces by Charge Accepting Adsorbates. *Angew. Chem., Int. Ed.* **2007**, *46*, 7315−7318.

(46) Wöll, C. The Chemistry and Physics of Zinc Oxide Surfaces. *Prog. Surf. Sci.* **2007**, *82*, 55−120.

(47) Pacchioni, G.; Cogliandro, G.; Bagus, P. S. Characterization of Oxide Surfaces by Infrared Spectroscopy of Adsorbed Carbon Monoxide: A Theoretical Investigation of the Frequency Shift of CO on MgO and NiO. *Surf. Sci.* **1991**, *255*, 344−354.

(48) Yang, C.; Yu, X.; Heißler, S.; Nefedov, A.; Colussi, S.; Llorca, J.; Trovarelli, A.; Wang, Y.; Wöll, C. Surface Faceting and Reconstruction of Ceria Nanoparticles. *Angew. Chem., Int. Ed.* **2017**, *56*, 375−379.

(49) Blyholder, G. Molecular Orbital View of Chemisorbed Carbon Monoxide. *J. Phys. Chem.* **1964**, *68*, 2772−2777.